Process simulation of fuel production through integration of high-temperature co-electrolysis in a Biomass-to-Liquid process

Benjamin Steinrücken[a], Marcel Dossow [a], Maximilian Schmid [a], Maximilian Hauck [a], Sebastian Fendt [a], Florian Kerscher [a] and Hartmut Spliethoff[a]

[a] Chair of Energy Systems, Technical University of Munich, Munich, Germany,
benjamin.steinruecken@tum.de

Abstract:

To reduce greenhouse gas emissions in the aviation sector, the development of so-called sustainable aviation fuel (SAF) is indispensable. SAF can be produced via different synthesis routes and has identical properties to fossil-based conventional aviation fuel. Based on the results of previous research, a process pathway to produce SAF via a Biomass-to-Liquid (BtL) concept using entrained flow gasification and Fischer-Tropsch synthesis is simulatively investigated. To optimize overall process efficiency, high-temperature co-electrolysis can be integrated into the process chain resulting in a Power-and-Biomass-to-Liquid (PBtL) approach. Co-electrolysis makes it possible to split carbon dioxide as well as water electrochemically in a single apparatus and to produce synthesis gas with the required properties for Fischer-Tropsch synthesis. A detailed 0D Python model of a reversible solid oxide cell (rSOC) was developed at the Chair of Energy Systems to calculate the steady-state fuel cell and electrolysis operation based on a defined input parameter set. The validation using measured and literature data shows that the current density-cell voltage behaviour can be reproduced with an average relative error of less than 5%. Based on the existing BtL process, two concepts for the integration of co-electrolysis are identified and the 0D rSOC model is integrated into the Aspen Plus® flowsheet simulation. The newly developed process options are compared with alternative PBtL process variants showing that an identical product yield and carbon efficiency is achieved in different configurations and that electrical power demand can be significantly reduced by integrating co-electrolysis.

Keywords:

Power-and-Biomass-to Liquid; rSOC; Sustainable Aviation Fuels; co-electrolysis.

1. Introduction

To defossilize the aviation sector sustainable ‘‘drop-in’’ fuels are the only realistic strategy. These so-called sustainable aviation fuels (SAF) can be produced via the biomass-to-liquid (BtL) route. Using lignocellulosic biomass such as carbon-neutral biomass residues as feedstock, the thermochemical BtL route is based on combining high TRL gasification technology with Fischer–Tropsch synthesis (FTS). However, such processes typically result in low system performance because the carbon efficiency η_c of the overall process is limited [1]. The main reason for this is the low H/C ratio in the raw biomass resulting in the necessity of carbon removal from the syngas after gasification to reach a molar H_2/CO ratio of about 2 suitable for FTS.

Electrification of the BtL route can help to overcome the overall η_c limitation of the BtL pathway. Indirectly or directly electrifying the BtL process, results in a hybrid process which not only aims at increasing the processes product yield PY per input biomass, but also presents a way to defossilize the energy intensive sectors such as aviation or maritime transport. Such Hybrid Power-and-Biomass-to-Liquid (PBtL) systems thus enable higher η_c than BtL routes at lower electrolysis requirements than pure Power-to-Liquid (PtL) alternatives. Additionally, the energy efficiency of the such a process is greater than that of the pure biomass-based ones, while being less sensitive on the electricity price than PtL processes.

In indirect electrification, providing additional H_2 from water electrolysis powered by renewable electricity makes it possible to overcome the η_c limitation of conventional BtL processes. This concept not only allows overall η_c close to 100% but also enables complete utilization of the electrolysis products as O_2 produced in electrolysis can be used for gasification [2]. Several studies exist on this indirect PBtL approach [3–9] .

In direct electrification, electricity can be used within one of the BtL process steps itself for supplying energy to the process. One promising option for direct electrification of the BtL process is the use of high-temperature co-electrolysis in the form of solid oxide electrolysis (SOEL). In co-electrolysis H_2O and CO_2 are split into H_2, CO and O_2 in one single step. This enables the targeted production of synthesis gas, which is

https://doi.org/10.52202/069564-0107

why co-electrolysis is an alternative for the WGS reactor used in the existing BtL process or the separate production of green hydrogen in the indirect PBtL approach. The integration of a SOEL into the process is facilitated by the fact that reforming reactions are catalysed internally due to the electrode materials [10]. Consequently, the purity requirements for the fuel gas are low compared to other electrolysis processes and an in-cell conversion of low hydrocarbons is possible.

There are few published studies that consider integration between gasification and co-electrolysis and even fewer that include FTS as the fuel synthesis step. Integrating co-electrolysis into a BtL process the SOEL can be in parallel to the BtL process chain, using a CO_2 stream separated from the syngas for example during acid gas removal. Samavati et al. investigated a such a PBtL process option using entrained flow gasification (EFG) coupled with co-electrolysis with FTS [11] and Zhang et al. compared a different PBtL concepts using either SOEL in co-electrolysis mode or hydrogen addition from SOEL featuring an EFG and producing SNG, MeOH, DME or SAF via FTS [5]. Using a CO_2 streams separated from the main syngas stream results in an increased partial pressure of the reactants and the total volume flow through the electrolysis can be reduced resulting in economic savings. The resulting process variants allow for increased PY and energy efficiency compared to pure BtL processes. A similar approach is taken in Nielsen et al. [12]. Here, the SOEL is integrated into a BtL process with FTS, using the volatile products from the FTS reactor as the inlet stream [12]. When compared with process variants in which H_2 is added to the process by water electrolysis, the power requirement of the process can be reduced as a result of co-electrolysis and increased energy efficiency can be achieved [12].

The main objective of this work is to demonstrate to what extent the integration of co-electrolysis is a way to efficiently electrify the BtL pathway. To this end, the operating mode of a SOEL is first modelled in Python and then integrated into the BtL Aspen Plus® process simulation using suitable integration concepts. The process variants are then evaluated and compared to those of Dossow et al. 2021 [8]. Apart from the evaluation of the integration concepts developed within the scope of this work, further development possibilities for the individual SOEL integration options are also shown in the following.

2. Fundamentals

2.1. Reference (P)BtL Process Description

The PBtL model framework into which the 0D rSOC model is integrated is based on the work of Dossow et al. [8] with their PBtL pathway serving as a reference case and is shown in Figure 1. The pretreatment of the lignocellulosic feedstock consists of a dryer and the dried biomass stream is fed to a torrefaction reactor. The solid so-called torrcoal produced has a high energy density and is ground in a downstream mill to a defined particle size of less than 300 µm [8]. To produce synthesis gas with a low methane and tar content from the torrcoal, an oxygen-blown EFG is used in the PBtL process. In addition to the thermodynamic modelling approach for CO, CO_2, H_2O, H_2 and CH_4, the formation of N-, S- and Cl-containing compounds is also modelled, assuming a carbon conversion of 99% [8]. In addition to the solid torrcoal, the gaseous by-product streams from the torrefaction reactor and the light-ends from FTS are fed to the gasifier [8].

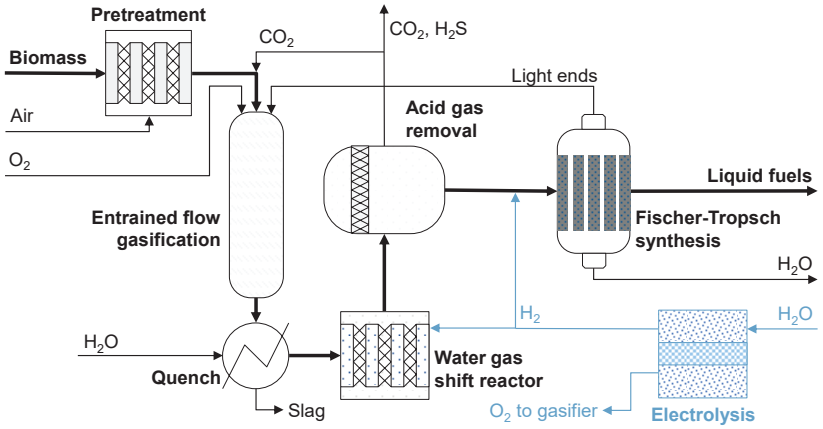

Figure 1. Schematic representation of the (P)BtL concept to produce SAF by Dossow et al. [8].

After EFG, slag and particles are removed, and the gas is abruptly cooled down by a water quench. Since halogen- and sulphur-containing impurities can lead to fouling in subsequent process steps or act as catalyst poisons, HCL is separated to a defined concentration by a chemically reactive filter system [8]. One of the key process parameters is the H_2/CO ratio of the synthesis gas. Typically, H_2/CO is below 1 directly after gasification and must be increased to a value of about 2 for the FTS. For this purpose, a sour WGS reactor

https://doi.org/10.52202/069564-0107

is used in the BtL process. It is assumed that the WGS reactor is operated isobarically and that the formation of H_2S and NH_3 is also catalysed in the reactor. The gas is then fed into an adsorption process that enables the separation of sulphur-containing components at high temperatures. The adsorbent used is ZnO, which is converted to zinc sulphide (ZnS) by a heterogeneous reaction. CO_2 is also removed from the synthesis gas in a downstream purification step. This is realised with the aid of a pressure swing adsorption (PSA) process, which is modelled in simplified form in the overall process. The products released in the process are removed from the process or, in the case of CO_2, partially used for pneumatic transport in the gasifier [8].

The synthesis gas prepared in the previous process steps is reacted in an FTS reactor at 230 °C and 20 bar using a cobalt-based catalyst. At the outlet of the reactor, the product stream is separated into a gaseous, an aqueous and an organic phase. The latter represents the crude fuel, which can be upgraded to SAF by a refinery process. The gas stream, which mainly contains unreacted synthesis gas and short-chain hydrocarbons, is fed into the FTS inlet stream or to the EFG via various recirculation routes. This can further increase overall η_c and PY [8]. The FTS reactor is modelled as a continuously operated stirred tank representing a slurry bed reactor. The reaction kinetics and product distribution are modelled using a macrokinetic model which is implemented as an object-oriented Python model using a FORTRAN subroutine that enables the exchange of calculation results between the two simulation environments [8].

In addition to the BtL process described above, Dossow et al. investigate different PBtL process variants. Here, an electrolyzer unit is integrated into the existing process and water is split into H_2 and O_2 which is then fed to the process. The electrolysers are assumed to be simplified stoichiometric reactors, with the product streams separated by a downstream separator [8]. An overview of the different PBtL process variants is provided in Table 1. Though the reference study contains both, PEMEL and SOEL, for comparison reasons in the following, only SOEL cases are considered.

Table 1. Indirect (P)BtL reference processes according to [8].

Process case	Description of the process modification
BtL case	Air separation is used to supply O_2 to the EFG. No electrolysis is used.
PBtL case 1	O_2 for the gasification is supplied from electrolysis instead of an air separation unit. The produced H_2 is fed partly to the WGS to adjust the H_2/CO ratio and partly to FTS.
PBtL case 2	No WGS to reduce complexity. H_2 is added to FTS to reach the desired H_2/CO ratio.
PBtL case 3	rWGS is used to convert CO_2 for maximum η_c H_2 is fed to FTS.

2.2. Solid oxide electrolysis (SOEL)

To substitute the WGS, a fuel electrode supported solid oxide electrolyser is chosen. A simplified model of the cell consists out of the supporting substrate layer, the electrolyte and the two electrode layers as shown in Figure 2.

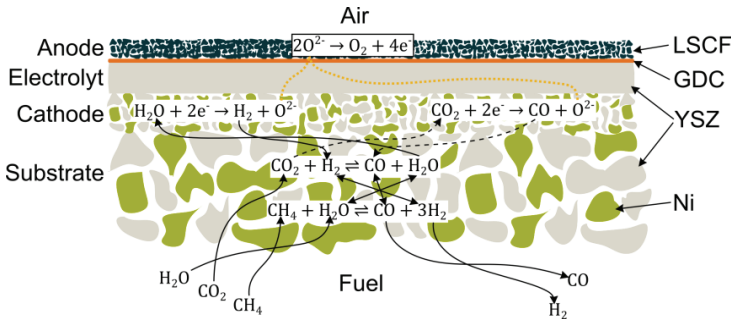

Figure 2. Schematic cross section of a solid oxide electrolysis with an internal reforming fuel.

The YSZ electrolyte is an O^{2-}-Ion conductor. The ions are created via the electrochemical reaction eq. 1 and eq. 2 under the consumption of electrons. These reactions are taking place at the triple phase boundaries where electrons from the electrically conducting nickel, Ions from the YSZ and gas from the porous layers meet.

$$H_2O + 2e^- \rightarrow H_2 + O^{2-} \quad (1)$$

$$CO_2 + 2e^- \rightarrow CO + O^{2-} \quad (2)$$

The simultaneous reduction of H_2O and CO_2 is referred to as co-electrolysis and, due to the catalysed side reactions, is based on a complex reaction network that has not yet been conclusively researched. Due to the high operating temperatures and the use of nickel, reforming and conversion reactions are catalysed on the surface of the fuel electrode in addition to the electrochemical reactions. The reaction equations for the steam reforming of methane eq. 3 and the reversed WGS reaction eq. 4 are given below, which take place when CH_4 or CO-containing fuel gas is fed to the fuel electrode. [13]

$$\mathrm{CH_4 + H_2O \rightleftharpoons CO + 3\,H_2} \qquad \Delta_R\bar{H}^0 = 206\,\frac{\mathrm{kJ}}{\mathrm{mol}} \tag{3}$$

$$\mathrm{CO_2 + H_2 \rightleftharpoons CO + H_2O} \qquad \Delta_R\bar{H}^0 = 41\,\frac{\mathrm{kJ}}{\mathrm{mol}} \tag{4}$$

These reactions take place in the substrate layer as well as in the fuel electrode layer. In addition to the already listed reaction equations, different pathways for the formation of CH_4 [14] or the separation of elemental carbon [15,16] are discussed in the literature. The extent to which the individual reactions are involved in the overall mechanism depends on the pressure and temperature as well as the process and material parameters due to the position of the reaction equilibrium [16–18]. To increase the efficiency of the SOEL, the O_2 generated on the anode side is discharged via a purge gas [16].

2.3. Electrochemical Model

The performance of the SOEL is calculated by subtracting the losses from the thermodynamically reversible cell voltage V_{Gibbs} calculated via eq. 6 by the global Gibbs Enthalpy difference of the reactions and the operational current J.

$$V_{Gibbs} = \frac{|\Delta G|}{J} \tag{5}$$

The global Gibbs enthalpy difference is calculated from the inlet and outlet streams via eq. 6.

$$\Delta\dot{G} = \dot{G}_{fuel,in} + \dot{G}_{oxy,in} - \dot{G}_{fuel,out} - \dot{G}_{oxy,out} \tag{6}$$

The operational voltage V_{op} of the electrolyser is calculated via eq. 7, by subtraction of the different loss mechanisms from the reversible cell voltage.

$$V_{op} = V_{gibbs} - \eta_{\mathrm{act}} - \eta_{ohm} - \eta_{diff} \tag{7}$$

The different loss mechanisms are included via over potentials: The activation over potential η_{act} is induced by the activation energy required for the electrochemical reaction. It is modelled with the Butler-Volmer formulation with a hyperbolic sine approach for fuel and oxygen electrode. The ohmic over potential η_{ohm} is induced by the temperature-dependent ohmic resistance of the electrolyte concerning the ion conduction and the constant contact resistance of the cell. The diffusion over potential η_{diff} models the loss mechanisms induced by the diffusion processes from the bulk phase to the electro-chemical reaction sites at the triple phase boundaries. These are modelled via Knudsen and binary diffusion for the fuel and the oxygen site. The bulk concentration is estimated via the mean over inlet and outlet concentrations with an inclusion of Methane and carbon monoxide for the hydrogen concentration. A complete description of the model used can be found in [19]. This recently updated model has been used in this work [20].

3. 0D rSOC Python Model

To meet the requirements of an open-source software solution with an simple syntax and object oriented paradigm, python coupled with Cantera is utilized for the thermodynamic equilibrium calculations. SOEL is still in the research and development phase (TRL<8), which is why the study results on co-electrolysis available in the literature are based on simulations or laboratory measurements on single cells or small stacks. In addition to the further development of the cell materials, the generation of synthesis gas is also the focus of research. The setting of the syngas parameters that is used to fuel the SOEL depends primarily on the composition of the inlet current and the location of the equilibrium of the WGS reaction. In addition, the current density has an influence on how much CO is formed.

3.1. SOEL Model

The calculation process of the SOEL model is shown in Figure 3: Both inlet gas streams are defined via their temperature, pressure, gas composition and flow rate. At the oxygen site, the temperature is increased to the operational temperature, the oxygen flow through the O^{2-}-Ions is added and in the last step the temperature is changed to the outlet temperature. At the fuel side after the temperature increase to operational temperature, an isothermal Gibbs reactor is positioned. Afterwards, the steam recycle stream is added and the electrochemical water splitting reaction takes place. The generated oxygen stream is removed and the chemical Gibbs equilibrium is formed. Afterwards, a portion of the stream is separated and recycled. In the last step, the temperature of the stream is changed to the outlet temperature. The steam recycle is required

https://doi.org/10.52202/069564-0107

to take the constantly ongoing water gas shift reactions in the cell into account. The positions of the Gibbs enthalpy for calculation of the global Gibbs enthalpy difference via eq. 5 are respectively marked.

To calculate the diffusion over potential, the partial pressures in the bulk phase are required. The inlet and outlet compositions x are used at the respective positions in the figure. For the over potential, the mean value between inlet and outlet is used. For the hydrogen diffusion, methane and CO are due to the water gas shift reaction and methane reforming considered as well.

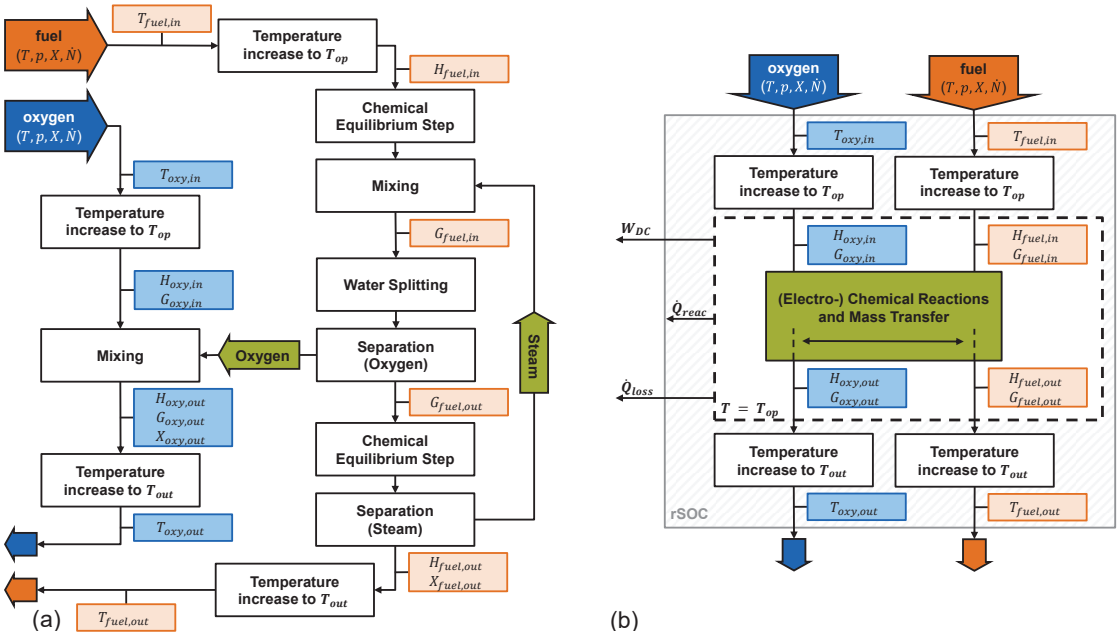

Figure 3. Calculation procedures of the SOEL model (a) and the energy balance (b).

All processes inside the SOEL model are isotherm at the operational temperature. Therefore, the energy balance is formulated via eq. 8.

$$\dot{Q}_R = \Delta\dot{H}_{oxy} + \Delta\dot{H}_{fuel} - W_{DC} - \dot{Q}_{loss} \tag{8}$$

The enthalpy difference of the inlet and outlet streams over the cell model, as well as the electrical power W_{DC}, heat losses $\dot{Q}_{loss}$ and the heat of reaction $\dot{Q}_R$ are considered. The positions for the enthalpy calculations of the streams are added into Figure 3.

3.2. Validation of the Python rSOC model

As described in [20], the parameters for the electrolyte activation energy and the electrolyte preexponential factor from [19] were optimized to fit experimental data. To validate the performance of the SOEL model for electrolysis and co-electrolysis operation experimental data is used [21]. The simulated data is compared to the experimental results for two different gas compositions in Figure 4.a). Gas composition A is a 50/50 H_2O/H_2, composition B is 25/25/25/25 $H_2/H_2O/CO/CO_2$. Both experiments were conducted at 770 °C.

The mean relative error of the SOEL mode is for the H_2/H_2O system 1.2 ± 1.2 % and for the co-Electrolysis operation with Gas B 0.5 ± 0.3 %. The accuracy of the model is reduced at higher current densities due to the increased influence of the diffusion losses. Due the usage of the mean concentrations over inlet and outlet for the bulk concentrations, nonlinear effects at low concentrations are not included. Besides the validated electrochemical performance of the cell, the fuel gas outlet composition of the electrolysis is crucial for a process integration. Hence, the outlet compositions for a relevant gas composition are validated as well, utilizing the experimental data from Schäfer et al. [15]. The model outlet concentrations are validated for an operation at 800 °C in a 10/60/30 $H_2/H_2O/CO_2$ gas composition. The comparison between the model and the experimental results by Schäfer are shown in Figure 4.b). For all gas species, an absolute error of the mole fraction of equal or below 0.02 is achieved. The accuracy of the model is high, expect for the methane concentration at high current densities. This relative high methane concentration at high current densities is discussed in Schäfer et al. [15], and is possible based on side reactions at the electrode. This phenomenon is still part of ongoing research.

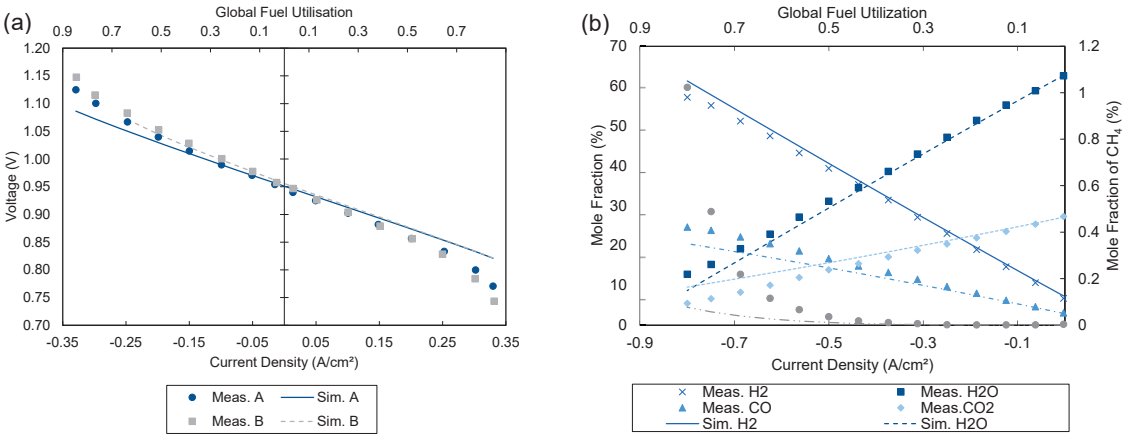

Figure 4. Validation of model performance with different fuels with experimental data [21] (a) and validation of the exhaust gas fractions in electrolysis mode with experimental data [15] (b).

4. PBtL Process Model using co-Electrolysis

The central objective of integrating co-electrolysis into the BtL process is to optimize and maximize the process in terms of PY, η_c, costs incurred and energy efficiency. For this purpose, the 0D rSOC model is integrated into the Aspen Plus® framework. Optimal points of integration of co-electrolysis into the BtL process are identified and suitable operational conditions are selected. To compare the different PBtL process options, a biomass inlet flow of 200 MW_{LHV} is assumed for all cases.

4.1. Integration of SOEL into PBtL Framework

The coupling between Python, FORTRAN and Aspen Plus® follows the procedure described in [8] as shown in Figure 5.a) For the integration of the rSOC into Aspen Plus®, a User2 model is used, as shown in Figure 5.b). This allows user-defined modelling of basic operations for any number of entry and exit streams. In addition to the material streams representing the entering and exiting fuel and O_2 streams, heat and work streams are also linked to the User2 block. Q-RSOC, Q-LOSS representing the heat of reaction and the heat losses that occur, and W-DC representing the required DC power, are calculated based on the energy balance solved within Aspen Plus®.

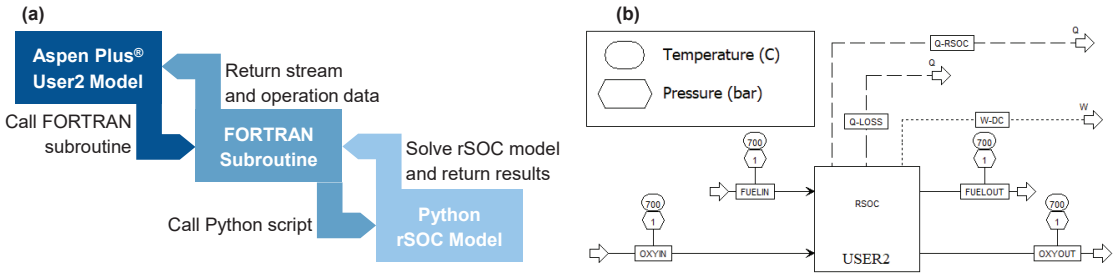

Figure 5. a) 0D rSOC Python model implementation in Aspen Plus® by using FORTRAN subroutine, b) Integration of subroutine into Aspen Plus® using USER2 model.

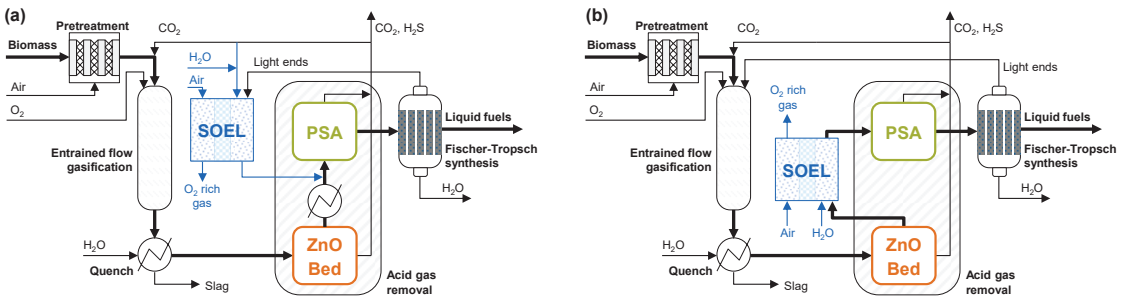

Figure 6. Process model for case I (a) and case II (b).

https://doi.org/10.52202/069564-0107

The SOEL makes it possible to produce H_2, O_2 and CO in one process step and to produce synthesis gas with defined properties. Thus, SOEL co-electrolysis offers an alternative to the WGS reactor as well as the additional feed of electrolytic H_2 as done in the reference PBtL process. For the PBtL concepts developed in this work, both, WGS and water electrolysis, can be dispensed. By removing the WGS reactor, the H_2/CO ratio of the synthesis gas required for the FTS must be adjusted with the help of co-electrolysis. The possible integration options are limited by catalyst poison and particle impurities in the raw syngas stream after gasification. If the SOEL is to be integrated into the main syngas stream, it must be located downstream of the ZnO bed and upstream of the CO_2 stream separation. At this point, the synthesis gas contains primarily H_2, CO, H_2O and CO_2 components. The catalyst poisons are removed down to very low concentrations <1 ppm. The corresponding process position is shown in Figure 6.a) and will be referred to as PBtL case I) in the following.

The SOEL makes it possible to produce H_2, O_2 and CO in one process step and to produce synthesis gas with defined properties. Thus, SOEL co-electrolysis offers an alternative to the WGS reactor as well as the additional feed of electrolytic H_2 as done in the reference PBtL process. For the PBtL concepts developed in this work, both, WGS and water electrolysis, can be dispensed. By removing the WGS reactor, the H_2/CO ratio of the synthesis gas required for the FTS must be adjusted with the help of co-electrolysis. The possible integration options are limited by catalyst poison and particle impurities in the raw syngas stream after gasification. If the SOEL is to be integrated into the main syngas stream, it must be located downstream of the ZnO bed and upstream of the CO_2 stream separation. At this point, the synthesis gas contains primarily H_2, CO, H_2O and CO_2 components. The catalyst poisons are removed down to very low concentrations <1 ppm. The corresponding process position is shown in Figure 6.a) and will be referred to as PBtL case I) in the following.

A second integration option is the insertion of a SOEL into the gaseous recycle stream of the FTS as shown in Figure 6.b). The FTS light ends primarily consist of unreacted H_2 and CO, as well as CH_4 and short-chain hydrocarbons, which can be converted to synthesis gas by the internally catalysed reforming reactions inside the SOEL. Since the corresponding material stream exits directly from the FTS reactor, the concentration limits for possible catalyst poisons are always met due to the upstream EFG. In this approach which locates the SOEL in parallel to the main syngas stream, the CO_2 contained in the main syngas stream after ZnO bed and SOEL is removed using a PSA. While part of the separated CO_2 is used as a carrier gas for the torrefied biomass at the gasifier section, the remaining CO_2 is recycled to the inlet fuel gas stream of the SOEL. This can increase η_c and PY. This PBtL case II) is similar to the approach of [12] for the integration of co-electrolysis into a BtL process with FTS. However, in the present work, as described at the beginning, the SOEL is used to adjust the H_2/CO ratio and, in contrast to [12], no additional WGS reactor is used.

4.2. Operational conditions of the SOEL

The SOEL are operated at atmospheric pressure and 800 °C. The active cell area and fuel utilisation are variable and defined in the simulation. The molar gas fractions are given in Table 2. The H_2S and HCl fractions are below ppm and thereby meet the quality requirements for the SOEL. Case II has non neglectable fraction of higher hydrocarbons in the range of C_2-C_4 from the FTS light end. Therefore, the risk of carbon formation for in case II is discussed in section 5.3.

Table 2. SOEL inlet gas fractions.

	H_2	H_2O	CO	CO_2	CH_4	C_{2-4}^{-}	$C_{2-4}^{=}$	HCl	H_2S
Case I	0.411	0.134	0.196	0.250	$8.69 \cdot 10^{-4}$	0.0	0.0	$8.30 \cdot 10^{-15}$	$8.08 \cdot 10^{-9}$
Case II	0.420	$1.72 \cdot 10^{-3}$	0.234	0.032	0.154	0.027	0.017	$1.90 \cdot 10^{-15}$	$9.25 \cdot 10^{-10}$

5. Results and Discussion

The PBtL cases I) and II) using co-electrolysis are evaluated in terms of operating parameters and possible heat integration. In addition, the occurrence of impurities and catalyst poisons as well as the formation of elemental carbon is considered.

The reference parameter used here is the syncrude produced in FTS, which is liquid at standard conditions (25 °C and 1 atm) and consists of a mixture of linear, saturated, and unsaturated hydrocarbons (mainly C5+). In addition to absolute parameters, such as the electrical power requirement or the raw syncrude or *fuel* mass flow produced, the focus of process development is on maximizing $PY = \dot{m}_{fuel} \cdot \dot{m}_{biomass,dry}^{-1}$, $\eta_c = \dot{m}_{C,fuel} \cdot \dot{m}_{C,biomass}^{-1}$, energy yield $EY = \dot{m}_{fuel} LHV_{fuel} \cdot \left(\dot{m}_{biomass} LHV_{biomass} + \dot{E}_{SOEL}\right)^{-1}$, and overall net energy efficiency $\eta_E = \dot{m}_{fuel} LHV_{fuel} \cdot \left(\dot{m}_{biomass} LHV_{biomass} + \dot{E}_{SOEL} + \dot{E}_{auxilaries}\right)^{-1}$.

5.1. Evaluation of the integration concepts

The operating behaviour of the SOEL can be influenced by the parameters FU and $\zeta_{CO_2,rcy}$. Suitable operating points for PBtL case I) are summarized for a fuel utilization between FU = 0.5 and 1.0 in Table 3. While U_Z increases only slightly between FU = 0.5 and 0.8, a very large increase is observed when comparing the cell stresses at FU = 0.9 and 1.0. This is due to mass transfer limitation because of high fuel utilization, which causes the over potentials to increase sharply. The ASR, whose value almost doubles for the two operating points starting from 0.25 to 0.47, confirms this assumption. $\dot{m}_{H_2O,SOEL}$ decreases with increasing FU, resulting in an overall lower total fuel flow entering the SOEL. As the inlet flow decreases, so does the area of the SOEL. Since the capital cost of a SOEL stack correlates with the area, this can be reduced because of operation at high fuel utilization. At this point, it should be noted that the conducted cell area determination is only a simple estimate for sizing the SOEL and shortening the computation time. For a comprehensive consideration of the integration concepts in the context of a techno-economic analysis, the choice of a constant active area is necessary.

Since the SOEL is directly integrated into the synthesis gas stream in PBtL case I), the product gas always exits with the same H_2/CO ratio of 2.10. This is not the case with integration at process position II). Here, the gaseous by-products of the FTS are reformed inside the SOEL and then recycled to the syngas stream. Since there is an H_2/CO ratio of about 1 at the outlet of the EFG, the H_2 content must be strongly increased in the used side recycle stream. Therefore, for the exemplary operating points investigated according to Table 3, a significantly higher H_2/CO ratio between 10.55 and 6.70 results, which decreases with increasing FU and $\zeta_{CO_2,rcy}$ and varies due to the composition of the FTS light ends stream.

At the operating points for PBtL case II), a larger additional water flow $\dot{m}_{H_2O,SOEL}$ enters the SOEL compared to case I). This is because the inlet fuel flow is coupled to the active area which decreases with increasing fuel utilization, whereas the supply of additional CO_2 leads to an increase. The ASR is determined to be a constant value of 0.20 for the simulated operating points regardless of the variable parameters FU and $\zeta_{CO_2,rcy}$. This indicates that no mass transfer limitations are simulated at a value of FU=0.9, which is confirmed by the slightly increasing values for cell voltage and DC power, respectively. The global fuel utilization is below the respective fuel utilization for the operating points investigated in the integration concepts. This serves as an input parameter in the simulation, and the difference between the two variables is due to the simplified modelling in co-electrolysis operation. To solve the energy balance around the SOEL, the inlet temperature of the oxygen stream is adjusted. This is limited by the maximum temperature level of the waste heat occurring in the process, which occurs at the exit of the EFG through a raw syngas cooler from 1400 °C to 1200 °C depending on the operating point. To ensure that the waste heat is also used efficiently in the integration concepts and that the temperature of the oxygen stream does not exceed the maximum limit, the mole flow at the oxygen electrode is increased as required for the simulated operating points. The ratio of oxygen and fuel mole flow is included in Table 3.

Table 3. SOEL parameters of selected operating points in PBtL cases.

Parameter	Unit	I.1	I.2	I.3	I.4	II.1	II.2	II.3	II.4
FU	-	0.50	0.80	0.90	1.00	0.50	0.50	0.90	0.90
$\zeta_{CO_2,rcy}$	-	-	-	-	-	0.50	0.90	0.50	0.90
U_Z	V	1.05	1.15	1.20	1.46	1.02	1.02	1.15	1.15
A_Z	m²	14545	13865	13629	13391	22895	27633	14331	15991
j	A/cm²	-0.41	-0.72	-0.83	-0.95	-0.50	-0.49	-0.90	-0.90
W_{DC}	MW_{el}	-63.0	-114.4	-136.4	-186.6	-117.5	-138.5	-148.9	-165.1
FU_{global}	-	0.37	0.65	0.76	0.87	0.46	0.45	0.82	0.82
ASR	Ω·cm²	0.22	0.23	0.25	0.47	0.20	0.20	0.20	0.20
$\dot{m}_{H_2O,SOEL}$	kg/s	6.31	5.42	5.12	4.78	22.47	25.75	14.08	15.16
$\frac{H_2}{CO}$	mol/mol	2.10	2.10	2.10	2.10	10.55	7.48	8.05	6.70
$\frac{O_2}{Fuel}$	mol/mol	1.00	1.00	1.00	1.00	1.50	1.50	1.50	2.00

5.2. Evaluation of the heat integration in the integration concepts

The indirect PBtL process variants developed by Dossow et al. are fully integrated with respect to the integration of the heat flows occurring within the process sequence [8]. The simulation results show that by using EFG, process heat is available at high temperature levels of over 1200 °C. In addition, the gasification, the WGS reaction as well as the FTS are exothermic process steps, whereby large heat flows are released.

https://doi.org/10.52202/069564-0107

These cover the required heat demand of the biomass pretreatment as well as the flue gas cleaning section. Based on the previous investigations, detailed modelling of the heat integration is omitted in this work. The integration of the SOEL into the process heat utilization is estimated using a $\dot{Q}$-T diagram.

For the PBtL case I), the $\dot{Q}$-T diagram representative for the operating point I.3 from Table 3 is shown in Figure 7.a). The curves show that despite the integration of the SOEL, sufficient process heat is available to cover the heat demand of the endothermic process steps. Starting from the maximum temperature level at 1293 °C, the heat is transferred between the occurring hot and cold heat flows. As can be seen from the graph, an excess heat flow of 116 MW_{th} remains at the cold end of the $\dot{Q}$-T diagram. This cannot be used within the process chain and must therefore be dissipated via additional cooling power to be expended. Since part of the waste heat is generated at an almost constant temperature level of approx. 230 °C, it could be used to generate process steam. The remaining heat flow must be removed from the process.

The $\dot{Q}$-T diagram of operating point II.4, which is shown in Figure 7.b), differs significantly from PBtL case I). Although the maximum temperature level of the waste heat present in the process is not exceeded, the curve of the cold heat flows plotted in blue is not completely below the red curve of the hot heat flows. As a result, assuming a minimum pinch point temperature difference of 10 K, additional process heat is required in the form of a cooling capacity of 112 MW_{th} and a heating capacity of 18 MW_{th}. The latter occurs at a very high temperature level of over 1235 °C and, with regard to the use of renewable energies, must be supplied with the aid of electricity or through the combustion of synthetic gases.

One possible reason for the increased heat demand is due to the high internal recycle ratio $\zeta_{CO_2,rcy} = 0.9$. As a result, the rWGS reaction, which is also endothermic, occurs in the SOEL in addition to the endothermic water electrolysis. To maintain the specified temperature difference across the SOEL of 0 K, the heat demand must be balanced by the enthalpy of the incoming oxygen gas stream. A large portion of the high-temperature process heat is transferred to this stream and the SOEL is heated to the operating temperature specified in the assumptions. Aa lower CO_2 recycle flow as well as the adjustment of the SOEL operating temperature can lead to a reduction of the high-temperature heat demand.

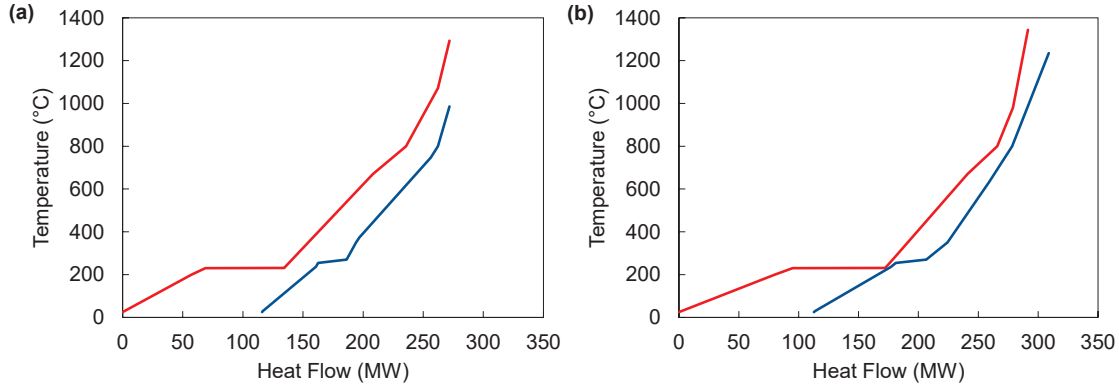

Figure 7. $\dot{Q}$-T diagrams of operating points I.3 (a) and II.4 (b) as a result of heat integration.

5.3. Discussion of the formation of carbon deposits

The SOEL is operated at 800 °C as part of the integration concepts. The risk of carbon deposition is investigated with a ternary diagram. On the fuel side, the recycle stream of the gaseous by-products of the synthesis FTS REC enters the SOEL hierarchy block. Its composition is within the carbon deposition region. With additional water and the CO_2 recycle stream defined by $\zeta_{CO_2,rcy}$ being introduced upstream of the electrolysis, the inlet composition at the SOEL is in a deposition free area. Despite FU = 0.9, the outlet composition is as well below the formation of carbon deposits. The integration into the FTS by-product stream requires a significantly higher H_2/CO ratio in the SOEL product gas to set the required syngas inlet parameters at the FTS reactor. At this point, it should be noted that in the FTS by-product stream, in addition to the unreacted syngas, the CH_4 and the short-chain hydrocarbons, long-chain, saturated and unsaturated hydrocarbons with more than four C atoms also occur in significant concentrations of several 100 ppm. These are not supported by the Cantera input file used in the simulation and are therefore considered inert in the rSOC Python model. In a real system, this is not the case. Here, the components are involved in the reactions taking place, and internal reforming of long-chain hydrocarbons is not possible. To prevent the rapid degeneration of SOEL, it is necessary to have an external pre-reforming step that converts the long-chain impurities.

https://doi.org/10.52202/069564-0107

5.4. Comparison with the Reference Processes

The influence of FU and $\zeta_{CO_2,rcy}$. on the overall process in terms of total electrical power demand, PY, and η_C for part of the operating points is shown in Figure 8. The electrical power requirement of the SOEL increases with fuel utilization. This determines the required electrical power in the overall process, with the additional auxiliary electrical power requirement ranging from 38.3 to 46.2 MW_{el}. With an increase in FU and $\zeta_{CO_2,rcy}$, PY increases and reaches a maximum value between 36.0% and 55.7% at operating point II.4. By incorporating co-electrolysis into the BtL process, the syngas composition can be influenced, and η_c can be more than doubles from 40.5% for the BtL process to 94.4% for the case II.4. Due to η_C and PY, operating points I.3 and II.4 are used for the comparison with the PBtL process variants according to [8].

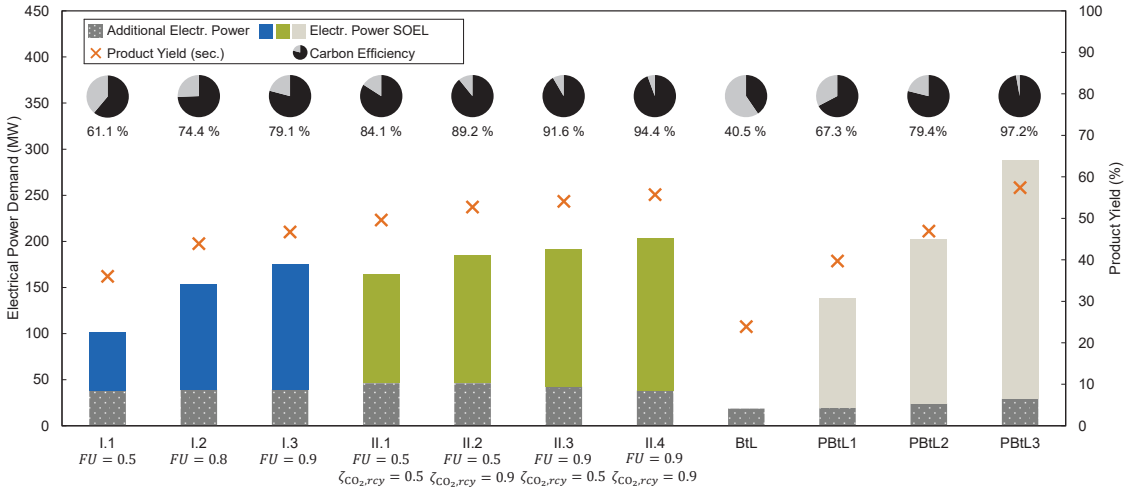

Figure 8. Overall process performance in terms of carbon efficiency, product yield and electrical power requirement for selected operating points of integration concepts I) and II) compared with the indircet (P)BtL process options according to Dossow et al. [8].

When comparing the different process options, it becomes clear how strongly the integration of electrolysis affects the electrical power requirement. While merely 18.7 MW_{el} is required for the BtL process, the value increases depending on the PBtL process variant up to a maximum of 287.4 MW_{el} for the indirect PBtL3 concept. The direct comparison of the integration concepts I.3 and II.4 with the PBtL process variants shows that almost identical product mass flows occur as for the indirect PBtL concepts 2 and 3. However, the power demand of the overall process can be significantly reduced by integrating co-electrolysis. The relative difference is 13.1% and 29.2% for the simulatively investigated cases I) and II), respectively.

Apart from the total electrical power P_{el} large deviations can also be observed in the inlet flows. The co-electrolysis concepts require more than three or four times the molar air flow than the indirect cases. The reason for this is the use of air as a purge gas for discharging the formed O_2 at the oxygen electrode of the SOEL. This is not considered in the PBtL process variants in Dossow et al. [8], so that only the air flow for the pretreatment of the biomass enters the process chain. It can be concluded that O_2 is produced in excess and cannot be further integrated into the process chain within the concepts presented here. When calculating the value, only the oxygen produced in the SOEL and consumed within the process chain is considered. The proportions in the purge gas used, if any, are not included. In addition to the air flow, the incoming hydrogen flow also increases in the integration concepts. This is due to an increased cooling demand in the quench section as well as the additional water flow to adjust the H_2/CO ratio. The latter is highly dependent on the SOEL operating point and can be reduced by adjusting the operating temperature and pressure.

It can be stated that by integrating co-electrolysis into the existing BtL process, large PY s as well as high η_c can be achieved, and the electrical power demand can be significantly reduced compared to the indirect PBtL process variants according to Dossow et al. [8]. A disadvantage is the high additional air and water flow required to operate the SOEL. To summarize to what extent EY and PY can be increased compared to the BtL concept, the relative deviations of both parameters with respect to the initial process are shown in Figure 9. While PY can be increased by up to 140% by incorporating electrolysis water or co-electrolysis, the increase in EY is lower at a maximum of 27%. However, this is strongly dependent on the respective process option, with values greater than 10% being achieved exclusively for the integration concepts developed in this work.

https://doi.org/10.52202/069564-0107

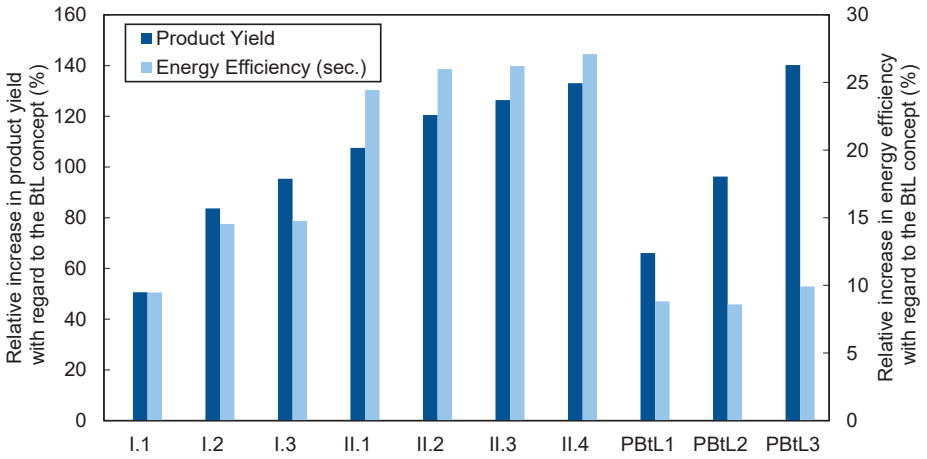

Figure 9. Relative increase in product yield and energy yield compared to the BtL process for the integration of co-electrolysis and the indirect PBtL process variants according to Dossow et al. [8].

6. Conclusion and outlook

To evaluate the suitability of the SOEL in co-electrolysis mode to enhance process efficiency of the BtL process, the newly developed 0D rSOC model is integrated into the existing simulation model. The SOEL replaces the WGS reactor and the additional feed of electrolysis hydrogen in the existing process chain. Two different process options are developed. In process option I, the SOEL is integrated into the syngas stream directly downstream of the ZnO bed, whereas in process option II the internally catalysed thermochemical reactions are used to reform the gaseous by-products of the FTS. In both cases, the SOEL is operated at 800 °C and 1 bar and optimized to set the necessary H_2/CO ratio for the synthesis. This is controlled by an additional water flow and the fuel utilization FU. In the integration concept II, the recirculation of the CO_2 stream separated in the EGR is also possible.

The simulation results of the developed process variants are compared with the PBtL reference processes from Dossow et al. [8]. In a first step, the influence of the fuel utilization FU assumed to be variable, and the CO_2 recycle ratio on the process parameters is investigated. The electrical power demand and PY increase with FU and CO_2 recycle ratio. A possible occurrence of carbon deposits is excluded with the help of the ternary diagram plot and the additional heating and cooling demand, if any, is estimated by a Q-T-diagram. The comparison with the PBtL process variants according to Dossow et al. [8] shows that an almost equal raw PY and η_c can be achieved in the integration concepts. The demand for electrical energy can be reduced by 27 MW_{el} and 84 MW_{el}, respectively, by integrating co-electrolysis for the simulative investigated operating points with an almost identical product flow. This corresponds to an increase in energy efficiency of up to eight percentage points, although the required air and water flow increases sharply. Nevertheless, the integration concepts developed in this work represent a promising alternative to the existing PBtL process variants due to the high product yields and the large potential savings in electrical power.

Numerous simplifying assumptions are made both in the creation of the Python rSOC model and in the integration of the SOEL into the BtL process. There is often the possibility to further develop the existing models and to increase their level of detail. For the Python rSOC model, the primarily concerns are the consideration of CO_2 electrolysis, which is neglected in the existing modelling approach, and the reduced accuracy at high fuel utilizations. Both issues can be addressed with an upgrade into a 1D model. Furthermore, the risk of carbon deposition for concept II is rather high, a more detailed investigation is required as well as the addition of a reformer prior to the SOEL. An investigation of the influence of the impurities at the SOEL to ensure a degradation free operation is required.

In simulative investigations of the integration concepts, constant SOEL operating parameters are assumed. Since these have a major influence on the position of the equilibrium of the internally catalysed reactions and therefore affect the product composition, the identification of an optimal operating range is conceivable. This could reduce the water and heating requirements as well as the associated costs. For a comprehensive comparison with the process variants according to Dossow et al. [8], a comprehensive heat integration as well as techno-economic analysis of the integration concepts is also required. In addition, it must be clarified how the O_2 rich purge gases can be further purified for use in the EFG.

7. Acknowledgments

The investigations have been supported by the Federal Ministry of Education and Research (BMBF) within the project REDEFINE H2E (01DD21005) which is gratefully acknowledged.

8. References

[1] Wenzel H. Breaking the biomass bottleneck of the fossil free society. CONCITO 2010.

[2] Agrawal R, Singh NR, Ribeiro FH, Delgass WN. Sustainable fuel for the transportation sector. Proceedings of the National Academy of Sciences of the United States of America 2007;104(12):4828–33.

[3] Bernical Q, Joulia X, Noirot-Le Borgne I, Floquet P, Baurens P, Boissonnet G. Integrated Design of High Temperature Steam Electrolysis and Biomass to Liquid Fuel Process. In: 11th International Symposium on Process Systems Engineering: Elsevier; 2012, p. 865–869.

[4] Hillestad M, Ostadi M, Alamo Serrano Gd, Rytter E, Austbø B, Pharoah JG et al. Improving carbon efficiency and profitability of the biomass to liquid process with hydrogen from renewable power. Fuel 2018;234:1431–51.

[5] Zhang H, Wang L, van herle J, Maréchal F, Desideri U. Techno-economic evaluation of biomass-to-fuels with solid-oxide electrolyzer. Applied Energy 2020;270:115113.

[6] Isaacs SA, Staples MD, Allroggen F, Mallapragada DS, Falter CP, Barrett SRH. Environmental and Economic Performance of Hybrid Power-to-Liquid and Biomass-to-Liquid Fuel Production in the United States. Environmental science & technology 2021;55(12):8247–57.

[7] Habermeyer F, Kurkela E, Maier S, Dietrich R-U. Techno-Economic Analysis of a Flexible Process Concept for the Production of Transport Fuels and Heat from Biomass and Renewable Electricity. Front. Energy Res. 2021;9.

[8] Dossow M, Dieterich V, Hanel A, Spliethoff H, Fendt S. Improving carbon efficiency for an advanced Biomass-to-Liquid process using hydrogen and oxygen from electrolysis. Renewable and Sustainable Energy Reviews 2021;152:111670.

[9] Pandey U, Putta KR, Rout KR, Rytter E, Blekkan EA, Hillestad M. Conceptual design and techno-economic analysis of biomass to liquid processes. Front. Energy Res. 2022;10.

[10] Dittrich L, Nohl M, Jaekel EE, Foit S, Haart LGJ de, Eichel R-A. High-Temperature Co-Electrolysis: A Versatile Method to Sustainably Produce Tailored Syngas Compositions. J. Electrochem. Soc. 2019;166(13):F971-F975.

[11] Samavati M, Martin A, Santarelli M, Nemanova V. Synthetic Diesel Production as a Form of Renewable Energy Storage. Energies 2018;11(5):1223.

[12] Nielsen AS, Ostadi M, Austbø B, Hillestad M, del Alamo G, Burheim O. Enhancing the efficiency of power- and biomass-to-liquid fuel processes using fuel-assisted solid oxide electrolysis cells. Fuel 2022;321:123987.

[13] Haart LGJ de, Beale SB, Deja R, Dittrich L, Duyster T, Fang Q et al. Forschungszentrum Jülich – Current Activities in SOC Development 2021.

[14] Nguyen VN, Blum L. Reversible fuel cells. In: Compendium of Hydrogen Energy: Elsevier; 2016, p. 115–145.

[15] Schäfer D, Fang Q, Blum L, Stolten D. Syngas production performance and degradation analysis of a solid oxide electrolyzer stack. Journal of Power Sources 2019;433:126666.

[16] Zheng Y, Wang J, Yu B, Zhang W, Chen J, Qiao J et al. A review of high temperature co-electrolysis of H2O and CO2 to produce sustainable fuels using solid oxide electrolysis cells (SOECs): advanced materials and technology. Chemical Society reviews 2017;46(5):1427–63.

[17] Foit S, Dittrich L, Nohl M, Vinke IC, Eichel R-A, Haart LGJ de. Understanding High-Temperature Electrolysis. ECS Trans. 2021;103(1):487–92.

[18] Peters R, Deja R, Blum L, van Nguyen N, Fang Q, Stolten D. Influence of operating parameters on overall system efficiencies using solid oxide electrolysis technology. International Journal of Hydrogen Energy 2015;40(22):7103–13.

[19] Hauck M, Herrmann S, Spliethoff H. Simulation of a reversible SOFC with Aspen Plus. International Journal of Hydrogen Energy 2017;42(15):10329–40.

[20] Hauck M, Schmid M, Herrmann S, Polat B, Steinruecken B, Poblotzki L et al. Modelling of an RSOC with Open Source Tools. European SOFC & SOE Forum Proceedings 2022:792–801.

[21] Preininger M, Stoeckl B, Subotić V, Schauperl R, Hochenauer C. Electrochemical Characterization and Performance Assessment of SOC Stacks in Electrolysis Mode. ECS Trans. 2019;91(1):2589–600.

https://doi.org/10.52202/069564-0107